

# Identification of optimal Sentinel-1 SAR polarimetric parameters for forest monitoring in Czechia

Daniel Paluba<sup>1</sup>, Bertrand Le Saux<sup>2</sup>, Francesco Sarti<sup>3</sup>, Přemysl Štych<sup>1,\*</sup>

<sup>1</sup> Charles University, Faculty of Science, Department of Applied Geoinformatics and Cartography, EO4Landscape Research Team, Czechia

<sup>2</sup> European Space Agency (ESA/ESRIN), Φ-lab – Climate Action, Sustainability and Science Department (EOP-S), Earth Observation Programmes Directorate, Italy

<sup>3</sup> European Space Agency (ESA/ESRIN), Earth Observation Programmes Directorate, Italy

\* Corresponding author: stych@natur.cuni.cz

## ABSTRACT

Time series analysis of synthetic aperture radar data (SAR) offers a systematic, dynamic and comprehensive way to monitor forests. The main emphasis of this study is on the identification of the most suitable and best performing Sentinel-1 SAR polarimetric parameters for forest monitoring. This is accomplished through: 1) a pairwise correlation analysis of SAR polarimetric parameters, multispectral optical vegetation indices and ancillary data, 2) a univariate binary time series classification for differentiation between forest types and 3) a visual exploration of time series. For this purpose, 600 validated broad-leaved and 600 coniferous forest areas in Czechia were used. Nine different SAR polarimetric parameters were examined, including VH and VV polarizations, VV/VH and VH/VV polarization ratios, the Radar Vegetation Index, Radar Forest Degradation Index, polarimetric radar vegetation index and the original and modified versions of the dual polarimetric SAR vegetation index. The pairwise correlation analysis revealed that most of the derived SAR polarimetric parameters were functions of each other with nearly identical behavior ( $r > |0.96|$ ). The strongest correlation of  $r \sim 0.50$  between SAR and optical features was found for broad-leaved forest for VV/VH and VH/VV. The highest overall accuracy in the time series classification of forest types was achieved by VH (76%), while for VV, VV/VH and VH/VV it was higher than 60%. Furthermore, the time series analysis of these parameters showed seasonal behaviors of the SAR features in both forest types. These results demonstrated the high relevance of using VH, VV, VV/VH and VH/VV time series in forest monitoring compared to other SAR polarimetric parameters. This study also introduces a novel pipeline to generate multi-modal time series datasets in Google Earth Engine (MMTS-GEE), used to generate data for the analysis. MMTS-GEE combines spatially and temporally aligned SAR and multispectral data, extended with topographic and weather data, and a land cover class label. Its high versatility enables its use in time series analyses, intercomparisons and in machine learning applications for tabular time series data. The GEE code for the proposed tool and analysis is freely available to the research community.

## KEYWORDS

time series; Google Earth Engine; SAR; time series classification; forest; Sentinel-2; Czechia

Received: 6 May 2024

Accepted: 24 October 2024

Published online: 4 December 2024

Paluba, D., Le Saux, B., Sarti, F., Štych, P. (2024): Identification of optimal Sentinel-1 SAR polarimetric parameters for forest monitoring in Czechia. *AUC Geographica* 60(1), 1–15

<https://doi.org/10.14712/23361980.2024.18>

© 2024 The Authors. This is an open-access article distributed under the terms of the Creative Commons Attribution License (<http://creativecommons.org/licenses/by/4.0>).

## 1. Introduction

Time series analysis of remote sensing (RS) data offers a dynamic and comprehensive way to monitor the Earth's surface and atmosphere in a systematic way. One of the most dynamically changing land cover types is vegetation, especially forests, being influenced by several anthropogenic and natural factors (Senf and Seidl 2021; Ma et al. 2023; Forzieri et al. 2022). Forest change is an important ecological process leading to reestablishment of forest biomass and structure (Bartels et al. 2016); therefore, incorporating time series in their monitoring is essential. Currently, the two most commonly used open-access RS data types are optical multispectral data (e.g., from Landsat or Sentinel-2 missions) and synthetic aperture radar (SAR) data (e.g., from the Sentinel-1 mission).

Optical vegetation indices, such as the Normalized Difference Vegetation Index (NDVI), Enhanced Vegetation Index (EVI), or biophysical and structural parameters, such as the Leaf Area Index (LAI) and Fraction of Absorbed Photosynthetically Active Radiation (FAPAR) are one of the most-known and most-used parameters for vegetation and forest monitoring in the optical domain (Zeng et al. 2022). NDVI is the most popular VI due to its simplicity, long history, and the fact that it can be created from the data of almost every RS sensor (Huang et al. 2021). EVI has improved sensitivity in high biomass regions compared to NDVI and it reduces the influence of the ground and atmosphere signal on the canopy response (Huete et al. 2002). LAI and FAPAR were identified as terrestrial Essential Climate Variables (ECV) by the Global Climate Observing System (WMO et al. 2011). These VIs are also generated on the global scale for operational use, e.g. NDVI and EVI from the MODIS or from NASA Visible Infrared Imaging Radiometer Suite (VIIRS) (at 250–1000 m and 16 days of spatial and temporal resolution, respectively) (Didan 2021b; 2021a; Didan and Barreto 2018), LAI and FPAR from MODIS and VIIRS (500 m and 4–8 days) (Myneni, Knyazikhin, and Park 2021; Myneni and Knyazikhin 2018), NDVI, LAI and FAPAR from the Copernicus Global Land Service (CGLS) (300 m and 10 days) (Fuster et al. 2020) or the Pan-European Sentinel-2 LAI, FAPAR and NDVI products (10 m and 1 day) (Smets et al. 2023).

Vegetation indices based on optical data are heavily dependent on sunlight, making them less effective in areas with frequent cloud cover. For this reason, SAR polarimetric parameters have also been developed for vegetation monitoring in recent years. They are based on a combination of backscatter coefficient from SAR polarizations, e.g. co-polarization ratios (PR) of VH/VV or VV/VH, Radar Vegetation Index (RVI), Radar Forest Degradation Index (RFDI), polarimetric radar vegetation index (PRVI), dual polarimetric SAR vegetation index (DPSVI) (Frison et al. 2018; Chang, Shoshany, and Oh 2018; Alvarez-Mozos et al. 2021; Hird et al. 2017; Kim and van Zyl 2000; Periasamy

2018; dos Santos, Da Silva, and do Amaral 2021) or incorporate also the phase information, such as the Dual-pol radar vegetation index (DpRVI) or the Compact-pol RVI (CpRVI) (Mandal et al. 2020a; 2020b). Compared to optical indices, which are altered primarily by physiological, biophysical, and biochemical changes in vegetation throughout the year, SAR signals can be strongly influenced not only by structural changes during the year but also by environmental factors such as precipitation and temperature (Olesk et al. 2015; Benninga, van der Velde, and Su 2019; Rüetschi, Small, and Waser 2019; Paluba et al. 2023). Environmental effects can alter the moisture content and, consequently, the dielectric properties of objects, which typically change throughout the year.

For the purpose of finding the most suitable combination of optical and SAR data for environmental monitoring, relationship/correlation between them has been evaluated. Moderate to high correlations were found between NDVI and SAR polarizations (VH and VV), polarimetric indices (Radar Vegetation Index – RVI, VH/VV, VV/VH and other) for crop monitoring, (e.g., in Alvarez-Mozos et al. 2021; Filgueiras et al. 2019; Holtgrave et al. 2020; Jiao, McNairn, and Dingle Robertson 2021) and interferometric coherence (Bai et al. 2020). However, these analyses were performed on an image-by-image basis and no time series data were included. Frison et al. (2018) were focused on the aspect of time series and a strong correlation between NDVI and the co-polarimetric ratio VH/VV for forest time series was found.

Effective computing platforms and algorithms are needed to assess, pre-process and test a wide range of data types, especially in time series analysis and machine learning approaches, such as classification or regression tasks. Current cloud-based platforms, such as Google Earth Engine (GEE), allow access to a wide range of datasets, as well as processing power in the cloud, without the need to download data locally or own high computational resources (Gorelick et al. 2017). The wide use of GEE is documented by recognized publication databases, such as the Web of Science (webofscience.com), where a total of 3,937 published contributions including the “Google Earth Engine” keyword in the abstract, title or keywords was found, while 1,032 were published last year, in 2023 (accessed on 16.7.2024). GEE has a prominent role in current forest monitoring efforts. The Global Forest Watch (Global Forest Watch 2014), using the power of GEE, collects global and regionally oriented forest datasets to provide deforestation (Reiche et al. 2021) or fire alerts (Tyukavina et al. 2022), map forest loss and gain (Hansen et al. 2013), primary forest distribution (Turubanova et al. 2018), forest greenhouse gas emissions (Harris et al. 2021) or identify the drivers of forest loss (Curtis et al. 2018) to mention a few.

Nowadays, there are about 400 RS datasets for deep learning applications, including Satellite Time

Series Datasets (Dufourg et al. 2024), as reported in Schmitt et al. (2023). These datasets contain data from various sensors and RS platforms, even their combinations, focusing on different topics, covering various geographical locations and time steps. Most of these datasets are mono-temporal, covering selected patches globally, but only for a single time step. Their publication dates vary, affecting the up-to-dateness of data, and their sizes range from a few megabytes to tens of terabytes. Although DL models trained on large geographic scales can work on local levels, their use in time series analysis for a defined area of interest would be challenging due to local specifics, time scale or equipped sensors.

For this purpose, in this work, a GEE pipeline to create multi-modal time series datasets (MMTS-GEE), specifically temporally and spatially paired labeled time series of S1, S2 and ancillary data (DEM and weather data), is developed. MMTS-GEE enables generation of paired time series for any time period (based on data availability) and over any geographic region as well as preprocessing data including cloud masking, speckle filtering and feature extraction. Selected and validated forest areas in Czechia were used to extract time series of selected SAR and optical indices/parameters, as well as ancillary data. The main goal and scientific contribution of this study is to identify the most suitable and best performing SAR polarimetric parameters for forest monitoring. It was accomplished through performing a pairwise correlation analysis of SAR, optical and ancillary data, time series classification in forest type differentiation and visual inspection of time series. The GEE code for the MMTS-GEE tool repository has been made available on GitHub to support open science.

## 1.1 Data

The main data sources for this study are Copernicus Sentinel-1 SAR data (S1) and Sentinel-2 multispectral data (S2) operated by the European Space Agency (ESA). The S1 C-band (with 5.405 GHz central frequency) SAR data in Ground-range detected (GRD) were accessed from GEE with a pixel size of 10 m and a spatial resolution of about  $20 \times 22$  m. Therefore, a spatial resolution of 20 m was used in all data processing in GEE and in further analyses. S1 data acquired before 2022 were used to explore the full potential of both Sentinel-1A and B satellites, which provided a 6-day temporal resolution until the end of 2021 when an anomaly occurred with the Sentinel-1B satellite (Pinheiro et al. 2022). The S2 mission with its two sun-synchronously orbiting satellites provides images of the Earth's surface in the optical domain every 5 days with a spatial resolution of 10, 20 and 60 m, depending on wavelength.

To enhance multi-modality and address the relationship between SAR backscatter and topographic

and climatic features, the Copernicus DEM digital elevation model (C-DEM) and weather data from the ERA-5 Land mission were also assessed. The C-DEM is a digital surface model representing the surface of the Earth, including buildings, infrastructure and vegetation for the time frame between 2011 and 2015 (European Space Agency and Airbus 2022). It is based on TanDEM-X satellite products provided by the German Aerospace Center (DLR) and Airbus Defence and Space. In this work, the C-DEM GLO-30 product was used, which represents a global DEM with a spatial resolution of 30 m. C-DEM was used to provide information on elevation, calculating slope, and local incidence angle (LIA). LIA, the angle between the look (incidence) vector of the SAR signal and the vector normal to the surface, was calculated for each S1 image separately based on the methodology of Paluba et al. (2021).

The ERA5-land is a reanalysis dataset from the original ERA5 dataset with an hourly temporal resolution and with an enhanced resolution of 0.1 arc degrees with a native resolution of 9 km (Copernicus Climate Change Service 2019, p. 5). The dataset includes 50 variables in an hourly step from 1981, from which two variables were used: "temperature\_2m", an average temperature of air 2 meters above the surface; and "total\_precipitation", accumulated liquid and frozen water, including rain and snow, that falls to the Earth's surface. The following meteorological data were derived from the ERA5 Land dataset for the selected study area: the sum of precipitation 12 hours prior to each SAR acquisition, and the temperature at the time of SAR acquisition.

Three land cover datasets, specifically ESA World-Cover v200 (ESA WC) for 2021 with a spatial resolution of 10 m (Zanaga et al. 2022), Corine Land Cover (CLC) for 2018 with a spatial resolution of 100 m and a minimal mapping unit of 25 ha (Kosztra et al. 2019), Copernicus Global Land Cover Layers Collection 3 (GLCL) (Buchhorn et al. 2020) with a spatial resolution of 100 m, and a forest-oriented dataset, the Hansen Global Forest Change v1.10 (GFC) with a spatial resolution of 30 m (Hansen et al. 2013) were used for forest mask generation.

## 1.2 Study areas and methods

### Study Areas

Czechia was selected as a case study. Czechia has a relatively high share of forests with heterogeneous species composition. In 2021, forests represented 34% of the total area of Czechia. The coniferous species represented 70% of the total forest cover, while the most populous species are *Norway spruce* (68% of all conifers), followed by pines (23%) and larch (6%). Broad-leaved species are represented mainly by beech (32% of all broad-leaved species), oak (27%) and birch (10%) (Ministry of Agriculture of the Czech Republic 2022).



### Automatic Forest Dataset Generation

Coniferous and broad-leaved forest areas were selected in the entire Czechia for this study. Healthy forest masks were created based on an enhanced pipeline from (Paluba et al. 2021; Onáčillová, Křištofová, and Paluba 2023), where an intersection of three land cover datasets (ESA WC, CLC and GLCL) and a forest-oriented dataset (GFC) was utilized. In the first step, pixels with a canopy closure greater than 50% in the base layer, as recorded in the GFC dataset for the year 2000, were selected. Pixels where a forest loss occurred between 2000 and 2021 (*forest\_loss* band) were further masked out. The CLC and GLCL datasets allowed differentiation between coniferous and broad-leaved forests; therefore, based on their intersection, broad-leaved and coniferous forest masks were created. Consequently, around 1000 random points with a 20-m buffer, entirely located inside the forest masks, were generated for the whole of Czechia for both forest types.

### Validation of automatically generated forest areas

In the next step, a verification of automatically generated healthy forest areas (~1000 from each class) was carried out to include only pure forest areas throughout the observed period. They were verified using a visual analysis with high-resolution images in Google Earth Pro (GEP). GEP provides satellite images with medium to very high spatial resolution, including providers such as NASA / USGS with Landsat data (30 m), CNES with SPOT data (10–1.5 m) or DigitalGlobe/Maxar with IKONOS and QuickBird data with sub-meter resolution (Bey et al. 2016). To differentiate between broad-leaved and coniferous forests, images that capture both leaf-on (summer) and leaf-off (winter) conditions of the forests were used. The *European Larch* (*Larix decidua*), a coniferous tree that loses its needles in autumn, was excluded from both the broad-leaved and coniferous input datasets to avoid discrepancies in the satellite time series.

To ensure that the areas did not undergo significant forest changes in 2021 and to eliminate possible errors introduced by the forest masks, only areas with at least 75% tree coverage in their 20 × 20 m buffered areas were left in the final input dataset. Areas located on the borders of different forest growth stages (small young versus high old trees) were excluded to avoid the effects of possible SAR shadowing on young trees caused by higher trees. Areas containing water or paved/concrete roads were also excluded. In the end, 600 coniferous and 600 broad-leaved forest areas were selected for further analysis. Their spatial distribution can be seen in Fig. 1.

### S1 and S2 Data Preparation and Pre-Processing

Initially, S2 Surface Reflectance (Level-2A) image tiles with cloud cover higher than 30% were filtered out (resulting in 871 S2 images for the entire Czechia in 2021). It should be noted that the S2 Level-2A data in GEE are already processed using the Sen2Cor processor and are automatically ingested to GEE from the Copernicus Open Access Hub (scihub.copernicus.eu). In the next step, the CloudScore+ approach, using the *cs* band with a default threshold of 0.60 was applied to exclude defected pixels affected by clouds, shadows and haze. CloudScore+ uses a weakly supervised deep learning approach to analyze the quality of each image pixel, while assigning per-pixel quality scores (Pasquarella et al. 2023; Pasquarella 2024). The *cs* band was used rather than the *cs\_cdf* due to its higher sensitivity to haze and cloud edges and is recommended for applications where an absolute clear pixel is required (Pasquarella 2024). A threshold of 0.60 was found to have sufficient tradeoff between masking the correct pixels and losing useful information in (Nicolau 2024). After the cloud unmasking, two optical vegetation indices, NDVI and EVI, and two vegetation parameters, LAI and FAPAR, were calculated. More information can be found in Tab. 1.

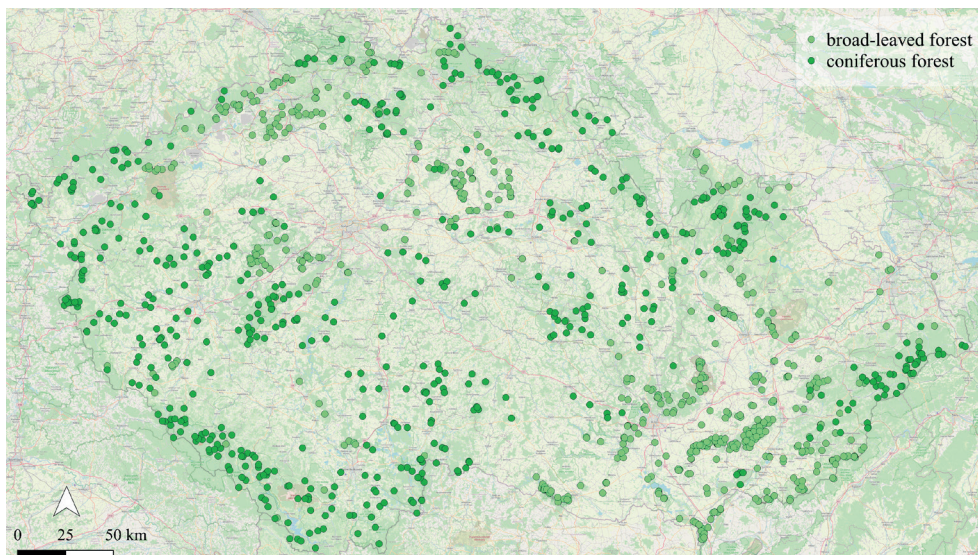


**Fig. 1** Spatial distribution of broad-leaved and coniferous forest areas used in this study.

**Tab. 1** Target optical vegetation indices.

Name	Abbreviation	Formula	Source
Normalized Difference Vegetation Index	NDVI	$\frac{NIR - RED}{NIR + RED}$	(Gamon et al. 1995)
Enhanced Vegetation Index	EVI	$2.5 \times \frac{NIR - RED}{NIR + 6 \times RED - 7.5 \times BLUE}$	(Liu and Huete 1995)
Leaf Area Index	LAI	based on (Weiss and Baret 2016)	*
Fraction of Absorbed Photosynthetically Active Radiation	FAPAR	based on (Weiss and Baret 2016)	*

Note: \* GEE implementation by Van Tricht (2023).

A total of 1,419 S1 images were acquired and pre-processed for the entire Czechia in 2021. Following Filgueiras et al. (2019), the Lee speckle filter with a window size of  $5 \times 5$  pixels was applied to the S1 data in GEE to reduce the speckle noise, based on the implementation in Mullissa et al. (2021). The Lee filter is one of the most used speckle filters, being computationally efficient while effectively smoothing the speckle effect and preserving the edges or subtle details (Lee 1985). The SAR polarimetric parameters (VV/VH, VH/VV, Radar Forest Degradation Index – RFDI, Radar Vegetation Index – RVI, the original Dual Polarized SAR Vegetation Index –  $DPSVI_o$  and its modified version  $DPSVI_m$ ) were then calculated in power/linear units (Tab. 2). The VV and VH polarizations were converted to decibels (dB), to a logarithmic scale.

### The final MMTS-GEE pipeline: Image pairing and time series data export

In the next step, the pre-processed S1 and S2 images were temporally and spatially joined and aligned. The joined S1–S2 image collection was created based on a spatial overlap and the 24-hour temporal difference

between the pre-processed S1 and S2 images. The S1 images served as master images in image stacking, that is, the S2 images were joined to the S1 images. The temporal difference of 24 hours was selected based on the findings that daily differences in optical VIs, e.g., in NDVI, are negligible (May et al. 2017). In total, 1254 S1–S2 pairs were identified in 2021 in Czechia. The analysis of temporal differences between the S1–S2 pairs resulted in a bimodal distribution. More than half of the pairs (643 images) had differences between 4 and 7 hours, while the second group of the pairs (611 images) had differences between 17 and 20 hours. The mean difference was 12 hours, with the majority of pairs having a difference of 5 (302 images) and 19 hours (288 images).

The ancillary features (DEM and weather data) were then calculated for each pixel and added to the feature space. At the end, an image collection was created, where each image includes spatially and temporally joined and aligned S1 and S2 images, topographic characteristics (elevation, slope, LIA) and weather data (temperature, precipitation). All data are resampled into a 20-m grid using the nearest neighborhood

**Tab. 2** Calculated SAR polarimetric features.

Name	Abbreviation	Formula	Source
Radar Vegetation Index	RVI	$4 \times \frac{VH}{VH + VV}$	[1,2]
Radar Forest Degradation Index	RFDI	$\frac{VV + VH}{VV - VH}$	[3]
Polarimetric Ratio 1	VV/VH	$\frac{VV}{VH}$	[4]
Polarimetric Ratio 2	VH/VV	$\frac{VH}{VV}$	[5]
Normalized Ratio Procedure between Bands	NRPB	$\frac{VH - VV}{VH + VV}$	[6]
Dual Polarized SAR Vegetation Index, original	$DPSVI_o$	$VH \times \frac{VV_{max} \times VH - VV \times VH + VH^2}{1.41421 * VV}$	[7]
Dual Polarized SAR Vegetation Index, modified	$DPSVI_m$	$\frac{VV_{max} - VV + VH}{1.41421 \times ((VV + VH)/VV) \times VH}$	[8]

References: [1]: Kim, van Zyl (2000), [2]: Sahadevan, Sitiraju, Sharma (2013), [3]: Saatchi (2019), [4]: Frison et al. (2018), [5]: Alvarez-Mozos et al. (2021), [6]: Hird et al. (2017), [7]: Periasamy (2018), [8]: dos Santos, Da Silva, do Amaral (2021)

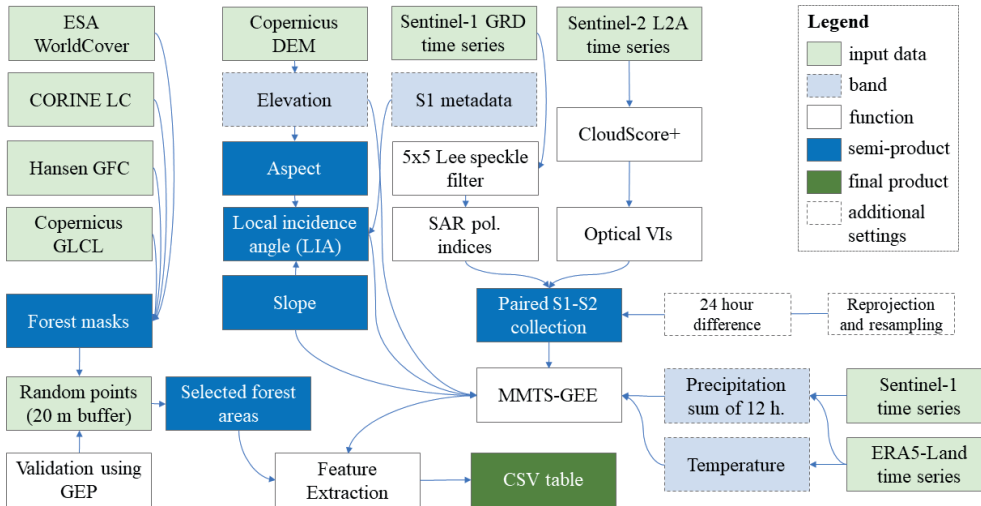


Fig. 2 Data pre-processing and preparation workflow of the MMTS-GEE.

method, while reprojection and resampling in GEE are done automatically on-the-fly.

Multimodal time series were extracted for each selected forest area. Each forest area had its unique ID and the date of SAR image acquisition. As the final step in GEE, each timestep-area combination including values of optical, SAR and ancillary features was exported from GEE in a csv table. The analysis was carried out using the original S1 coordinate system for Czechia (EPSG:32634) and with a spatial resolution of 20 meters, which matches the spatial resolution of the S1 data. The full pipeline of the MMTS-GEE is depicted in Fig. 2.

### Pairwise correlation analysis of optical, SAR and ancillary features

In the next step, a pairwise correlation analysis was performed between each SAR feature, to assess similarities between them and to reduce possible data redundancy by excluding features. The second correlation analysis focused on exploring the relationship between SAR features and optical features generated from S2 data. For these analyses, all exported data were used, that is, each time step for each selected point. Pairwise correlation analysis was performed and a Pearson's correlation coefficient ( $r$ ) was calculated for each combination of features.

To examine seasonality in the optical and SAR domains for both forest classes, a time series analysis was performed on the entire input dataset (600 for each class). Additionally, the mean value for each time step was calculated separately for each class to obtain a complete understanding of the seasonality for each class.

### Time series classification on forest type differentiation

To examine the performance of each individual SAR polarimetric parameter (Tab. 2) and both polarizations of S1, a univariate time series classification (TSC) was performed using the Time Series Support Vector Classifier (TS-SVC). The TS-SVC was specifically adopted

for time series analysis and is available from the *sktime* Python library (Löning et al. 2022). As the exported time series are based mainly on the availability of S2 data, they are unequal in length for different areas in Czechia. They were first imported into a Python environment and prepared in a Pandas multiindex format (with 'date' and 'ID' as indices), as expected by the *sktime* algorithms. The TS-SVC was selected as the only classifier in the *sktime* library to deal with unequal lengths of time series. Moreover, TS-SVC is considered to be one of the most used algorithms for TSC tasks, while in some cases achieving superior accuracy (Wang et al. 2022; Faouzi 2022). The Radial Basis Function (RBF) was selected as a kernel type due to its general good performance for SVC in RS applications (Thanh Noi and Kappas 2018; Mountrakis, Im, and Ogole 2011; Oliveira, Dutra, Sant'Anna 2023). To find the best performing regularization parameter  $C$ , fine-tuning of 11 different values (0.1, 1, 5, 10, 50, 100, 150, 200, 300, 500 and 1000) was performed for VH polarized time series in differentiation between coniferous and broad-leaved forests.

After finding the best  $C$  parameter, a univariate time series classification was performed for each S1 SAR polarization and polarimetric parameter (Tab. 2), and the overall accuracy (OA) was calculated. Forest areas were divided into training and testing samples. Time series of 70% of points of each forest type was used in training the TS-SCV, while the remaining 30% was used to test the accuracy for various  $C$  parameters and also in accuracy assessment of various SAR features.

## 2. Results

### 2.1 Pairwise Correlation Analysis

To explore the proposed SAR polarimetric parameters and other features derived from DEM and weather datasets, a pairwise correlation analysis was performed in the first step. In general, pairwise



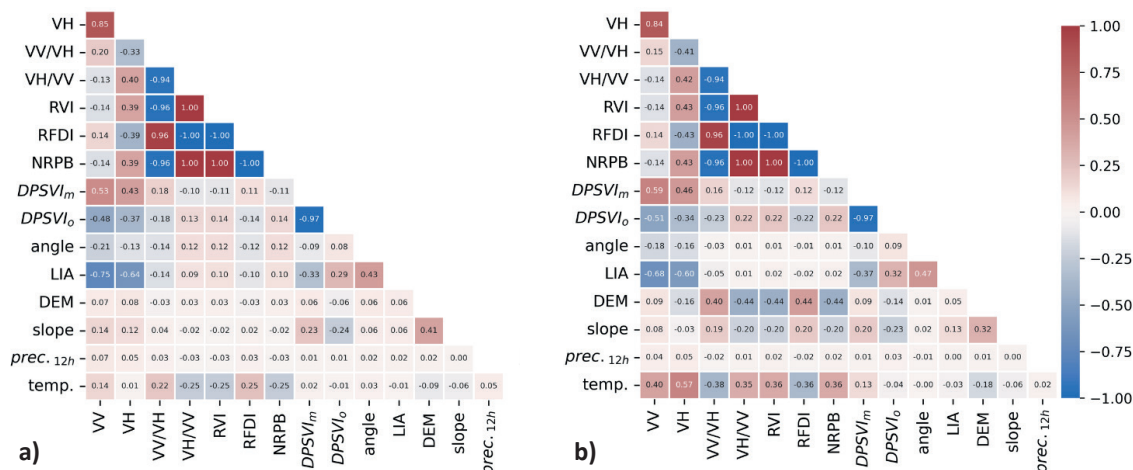


Fig. 3 Pairwise correlation between SAR, DEM and weather features for a) broad-leaved (n = 17303) and b) coniferous forest areas (n = 13070).

correlation analysis indicates a consistent pattern of correlation between certain features for both forest types, while there are features suggesting that some features interact differently for different forest types. A perfect negative or positive correlation ( $r = +/ -1.00$ ) was found for each combination between VH/VV, RVI, RFDI and NRPB for both broad-leaved and coniferous forests (Fig. 3a and Fig. 3b), meaning that they are functions of each other. They also had a very high correlation with VV/VH ( $[0.94] - [0.96]$ ) and a moderate correlation with VH ( $\sim |0.40|$ ), while the correlation with VV was low ( $\sim |0.15|$ ). The VV/VH and VH/VV had a mutual correlation of 94%, while they had slightly different correlations with other examined features. The  $DPSVI_o$  and its modified version ( $DPSVI_m$ ) had a mutual correlation of  $-0.97$  for both forest types, while having a moderate correlation with VV and VH and a low correlation with other SAR parameters.

As expected, a high correlation ( $-0.60 - -0.75$ ) was found between the LIA and VV and VH polarizations, being stronger for broad-leaved forests, while the SAR parameters had almost no correlation with LIA.

The temperature had a moderate correlation with the polarimetric parameters ( $0.35 - 0.38$ ) and with VV and VH polarizations ( $0.40$  and  $0.57$ , respectively) for coniferous forests. The correlation for broad-leaved forests was about  $0.25$  between temperature and SAR features and very low for VV and VH polarizations ( $0.01$  and  $0.14$ , respectively). On the other hand, precipitation showed almost no correlation with SAR or other features. DEM features, slope and elevation, were moderately correlated with polarimetric features only for coniferous forests, while for broad-leaved forests they exhibited almost no correlation.

The pairwise correlation in Fig. 4 demonstrates the varying relationships between SAR and optical features in different forest types. A stronger linear relationship ( $\sim 0.50$ ) was found for the polarimetric parameters VV/VH and VH/VV in broad-leaved forests compared to coniferous forests. However, coniferous forests exhibited stronger correlations of both S1 polarizations with LAI and EVI. FAPAR achieved the strongest correlation between SAR and optical features for broad-leaved forests, while for coniferous forests it exhibited almost no correlation (Fig. 4b).

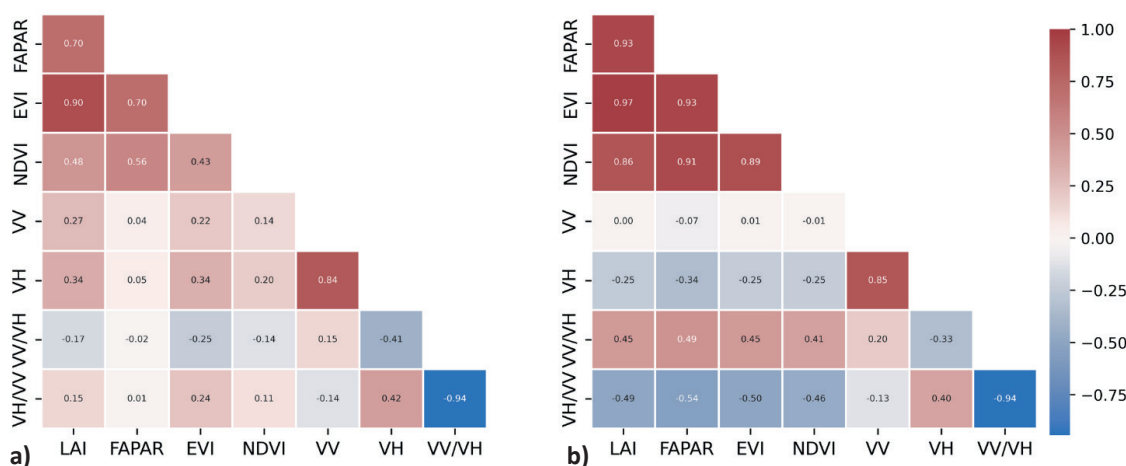


Fig. 4 Pairwise correlation between SAR and optical features for a) broad-leaved (n = 17303) and b) coniferous forest areas (n = 13070).

The strongest correlation for coniferous forests of each SAR feature was found for EVI.

The analysis also shows the correlation between each individual optical vegetation indices and parameters. Generally, the strongest correlation was found for broad-leaved forests: over 0.85 for each combination and a maximum of 0.97 between EVI and LAI. Coniferous forests exhibited a moderate correlation between NDVI and other optical features ( $\sim 0.50$ ), while the highest correlation was also achieved between EVI and LAI.

Based on the results of the pairwise analysis, some of the tested SAR features (RVI, RFDI, NRPB, and VH/VV) showed perfect correlation with each other; therefore, RVI, RFDI, and NRPB were excluded from further analysis, while VH/VV was retained.

## 2.2 Time series analysis

Generally, optical vegetation indices and parameters were higher in magnitude for broad-leaved forests in summertime and lower in wintertime compared to coniferous forests, while coniferous forests exhibited a more stable pattern throughout the year. Time series analysis of optical features, showed a clear and expected seasonal pattern for broad-leaved forests with low values in the beginning of the year, peaks in mid-year/summertime and a decrease in late spring with the lowest values during wintertime (Fig. 5a). The optical time series for coniferous forests shows a similar seasonality with peaks in summertime for

EVI and LAI (Fig. 5b and 5c) and a rather stable behavior throughout the year with a slight increase toward winter for NDVI and FAPAR (Fig. 5a and 5d). Some areas represent some noise throughout the year, even in the summertime. The lack of data in the wintertime is apparent in the time series, causing a rather noisy behavior of the signal with high fluctuation, especially in NDVI and FAPAR. Certain variability in individual time series, represented by the lighter lines in Fig. 5, can be detected within each forest type.

In the case of SAR time series, clear seasonal behavior was found in both polarizations and ratios (VV/VH and VH/VV) for both forest types, while  $DPSVI_o$  and  $DPSVI_m$  exhibited a rather noisy behavior throughout the year (Fig. 6). The more apparent differentiation between forest types is enabled by VH polarization and both ratios, while VV showed similar behavior and values for both forest types. The seasonalities found for these features are opposite in nature for the two forest types. For example, the VH backscatter and the VH/VV increase in summertime for coniferous forests, whereas they decrease for broad-leaved forests. An opposite behavior can be observed in VV/VH, which decreases in summertime for coniferous forests and increases for broad-leaved forests. In contrast, VV increases in wintertime for both forest types. Overall, higher values were obtained in the VV polarization compared to those obtained in VH. Higher variation in individual time series can be observed for SAR features compared to optical parameters.

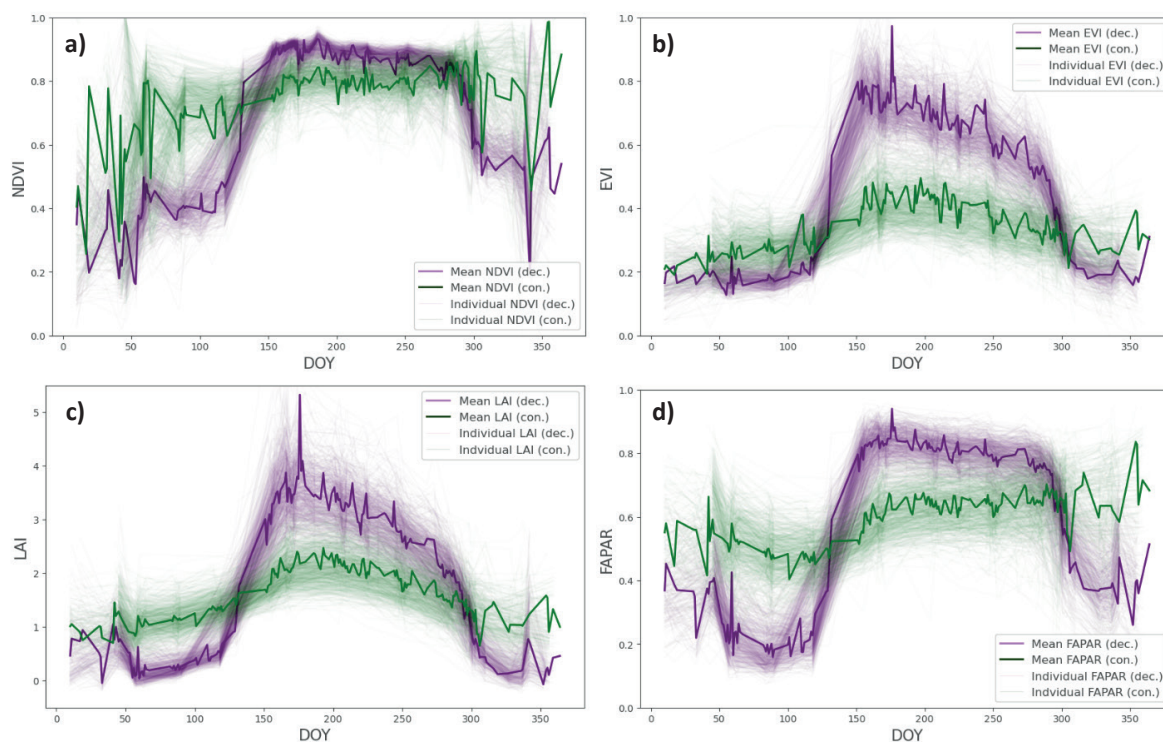


**Fig. 5** Average and individual time series for 2021 of a) NDVI, b) EVI, c) LAI and d) FAPAR using all input data for broad-leaved and coniferous forests.

Note: *dec.* = deciduous forests, *con.* = coniferous forests



### 2.3 Time series classification

Fine-tuning the TS-SVC model, especially the C parameter yielded expected results: the overall accuracy is increasing with increasing of the C parameter value. An increase from 0.1 to the default C parameter for TS-SVC in sktime ( $C = 1$ ) showed an increase in OA of 22%. The further increases in OA were slighter, that is, by 2.5% from 1 to 5 and by 0.8% between 5 and 50, 50 and 100 (Fig. 7a). The best OA, 76.12% were achieved with  $C = 200, 300$  and 500, while another increase to 1000 resulted in a decrease of 0.3% in OA (Fig. 7a). This suggests that increasing the C parameter above 200 does not improve the accuracy of the model. For this reason, 200 was set for the regularization parameter C and used in the comparative analysis of the performance of each individual SAR polarization and polarimetric parameter in the differentiation between forest types.

The results of the TSC indicate the highest OA for VH polarization with 76.12%, significantly outperforming other SAR features by at least 11%. The second highest OA was achieved by VH/VV (65.73%), followed by NRPB and RFDI (both 64.89%). Accuracies over 60% were achieved also by VV, VV/VH and RVI (Fig. 7b). Based on the pairwise correlation analysis, where NRPB, RFDI, RVI, and VH/VV each demonstrated a 100% correlation with each other (Fig. 3), VH/VV was identified as the most promising SAR polarimetric parameter for forest monitoring among these four; due to its highest OA in the TSC. The lowest accuracies below 60% were achieved by DPSVI<sub>m</sub> and DPSVI<sub>o</sub> (53.65% and 47.19%, respectively). These results indicate that the DPSVI indices are less capable of discriminating between forest types. Furthermore, based on the SAR time series analysis (Fig. 6), these features showed a rather noisy behavior throughout the year, which explains the lower accuracy achieved in TSC.

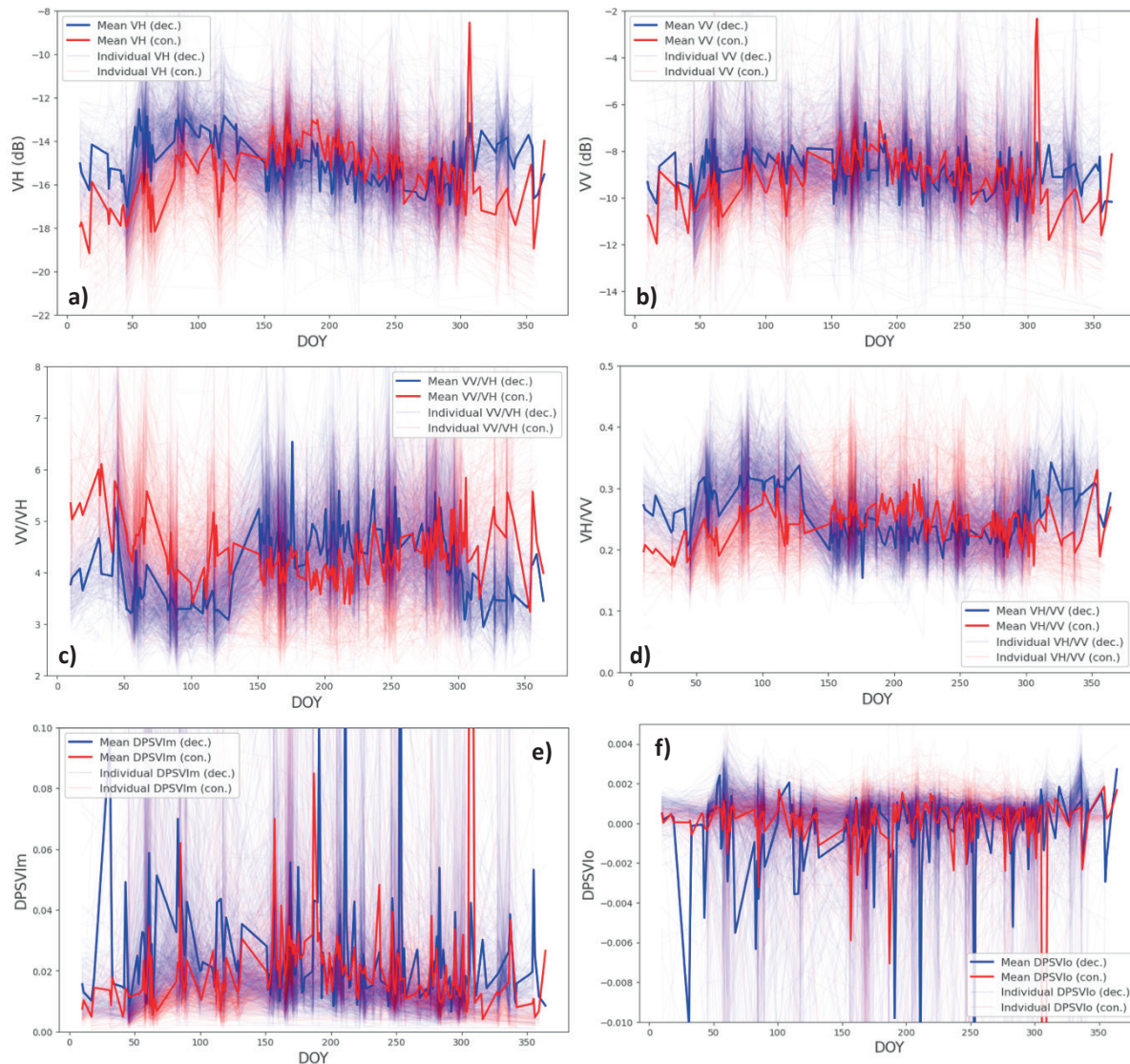


**Fig. 6** Average and individual time series of a) VH, b) VV, c) VV/VH d) VH/VV, e) DPSVI<sub>m</sub> and f) DPSVI<sub>o</sub> using all input data for broad-leaved and coniferous forests.

Note: *dec.* = broad-leaved forests, *con.* = coniferous forests

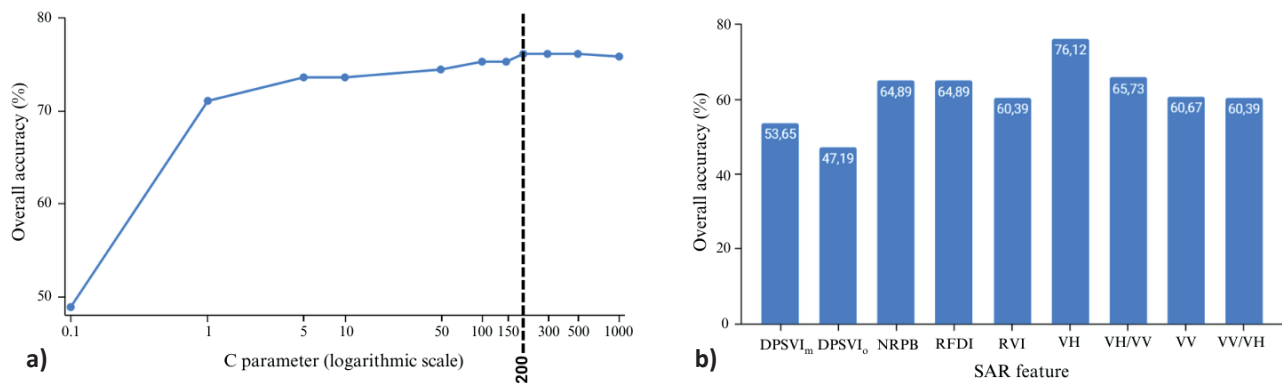


**Fig. 7** Fine-tuning of the C parameter for the TS-SVC (a) and results of TSC for SAR polarizations and polarimetric parameters (b).

Therefore, the final selection of the best performing SAR features based on each analysis was VH, VV, VH/VV and VV/VH.

#### 2.4 The MMTS-GEE dataset generation tool

The proposed MMTS-GEE tool, which generates a temporally and spatially paired time series dataset of S1, S2, DEM and weather data, has several parameters, which the user can set to customize the area of interest, time range, the preprocessing pipeline or export settings. The following settings can be set in the GEE environment:

- Time series length: Set the start and end dates to generate time series.
- Random point generation: If enabled, users can specify the type of land cover from the ESA World Cover 2021 to generate random points, the number of these points, and a buffer around each point. Alternatively, users can import their own spatial data as a GEE FeatureCollection and use it in time series generation.
- Geographical coverage: Select a broad geometry like an entire country or manually draw a custom ROI, needed for the initial data assessment.
- Sentinel-2 data preprocessing: Settings to adjust the CloudScore+ algorithm settings for cloud unmasking are available.
- Optical and SAR indices: Choose from a list of predefined optical and SAR polarimetric indices to include in the output.
- Speckle Filtering: There is an option to perform speckle filtering on SAR data using a Lee filter, with configurable kernel window size.
- S1–S2 temporal difference: Set the temporal difference between the S1 and S2 images when pairing them temporally can be set.
- Null Value Handling: Decide how to handle null values in the exported data, with options to exclude all rows with nulls, include only rows where optical indices have nulls, or include all nulls.

It should be noted that the MMTS-GEE code is freely available, therefore, other settings, not included in

the recommended user settings listed above, can be adjusted by editing the code. To list a few, users can create their own optical or SAR indices, select a different land cover database for random point generation, set a different speckle filtering approach, or integrate other ancillary data to enhance the multi-modality of the created time series dataset.

### 3. Discussion

In this study, a tool for creating multi-modal time series datasets, consisting of spatially and temporally aligned and paired preprocessed S1, S2, weather and DEM data was created in GEE (MMTS-GEE). The MMTS-GEE tool is unique because it enables generation of paired time series for any time period (based on data availability) and over any geographic region, both locally and globally. Moreover, customization of data preprocessing pipelines, including cloud masking, speckle filtering and feature extraction, or further extension with other ancillary datasets is possible. This versatility addresses various challenges of the currently used satellite-based datasets, as presented in Schmitt et al. (2023). Therefore, the GEE code for the MMTS-GEE tool has been made publicly available in the GitHub repository of this work at [github.com/palubad/MMTS-GEE](https://github.com/palubad/MMTS-GEE). In the present form, the MMTS-GEE is prepared for export of tabular data, but the next work will focus on improving the MMTS-GEE to export image patches for deep learning (DL) analyzes to fully address the requirements for DL analysis in (Schmitt et al. 2023).

The testing and evaluation of various SAR polarimetric parameters was performed to select the most suitable ones for forest monitoring using both quantitative (pairwise correlation analysis and TSC) and qualitative analysis (time series comparison). For this, time series were generated for 600 broad-leaved and 600 coniferous areas using the MMTS-GEE. Based on the pairwise analysis of mutual correlation between SAR features and the highest achieved OAs in TSC on differentiation of forest types, four SAR features were considered as the most suitable and best performing

ones for forest monitoring: two original S1 polarizations VV and VH and two most commonly used polarization ratios VV/VH and VH/VV. Some of the tested SAR features were excluded due to a perfect correlation between each other (RVI, RFDI, NRPB), while a perfect correlation between RVI and RFDI was also found in Paluba et al. (2023). This suggests that these indices are functions of each other and did not provide new information.  $DPSVI_m$  and  $DPSVI_o$  were excluded from the final selection due to their low accuracy in TSC and their rather noisy time series behavior for both forest types. Although a high correlation was also found between the VV and VH polarization (0.84–0.85), they were included in the final selection of the most efficient SAR features. With that, the original polarizations of the S1 data were preserved. Moreover, VH polarization achieved the highest OA in TSC, suggesting that it is the most reliable and important SAR feature to distinguish between forest types and for forest monitoring in general.

The basic assumption based on previous studies (Dostálová et al. 2016; Frison et al. 2018), that SAR feature time series have seasonal variations for forests, was confirmed (Fig. 6). Seasonal variations in SAR backscatter have been observed in both coniferous and broad-leaved forests, although their seasonality differs. Coniferous forests exhibit increased backscatter in VV and VH in summer and reduced backscatter during colder conditions, often attributed to loss of moisture content, needle loss and the presence of understory vegetation, which can be formed by broad-leaved plant types (Dostálová et al. 2016; 2018; 2021). Broad-leaved forests, on the other hand, show higher VV and VH backscatter values during leaf-off periods due to decreased attenuation by tree crowns, particularly by leaves with sizes similar to or larger than the C-band wavelength (~5 cm). This leads to a higher received backscatter resulting from multiple scattering between primary and secondary branches, or even between the tree trunk and the ground, depending on tree crown density. Lower backscatter values during hot and dry summer days are associated with a reduced moisture content in vegetation, allowing greater penetration of the SAR signal into the tree crown and less backscatter returning to the SAR sensor. Generally, higher backscatter values are obtained for VV polarization in both forest types, confirming previous findings (Dostálová et al. 2016; 2018; Paluba et al. 2021). A clearer and more distinct seasonality in the VH polarization for both forest types compared to VV can be attributed to the fact that the VH polarization is more strongly affected by volume scattering (Richards 2009; Vreugdenhil et al. 2018). The lower number of observations from wintertime caused a rather noisy behavior, similarly as in optical features. The lack of data in wintertime in the case of SAR data is due to the fact that only unmasked paired S1–S2 observations were considered in the analysis, therefore the number of S1 observations is equal to

the number of valid/unmasked observations by S2. Overall, the analysis of these SAR parameters suggests that the SAR backscatter is sensitive to seasonal changes in forest composition.

Topographic properties can significantly alter the backscatter behavior over time, especially when SAR images are combined from ascending and descending orbits (Paluba et al. 2021). A high correlation between the LIA and both S1 polarizations for both forest types can be caused by the fact that the input time series included S1 data derived from every possible acquisition geometry, i.e., both from ascending and descending orbits with variations in LIAs for the same area. The moderate correlation of DEM features (slope and elevation) with SAR features for coniferous forests and almost no correlation for broad-leaved forests can be attributed to the topographical distribution of the input areas. Broad-leaved forest areas had a mean elevation of 417 m with a range of 823 m, while the mean for coniferous forests was 650 m with a range of 1119 m.

Environmental effects, such as precipitation, alter moisture content and consequently the dielectric properties of objects, which typically change throughout the year (Rüetschi, Small, and Waser 2019; Benninga, van der Velde, and Su 2019; Ranson and Sun 2000). However, precipitation had almost no correlation with S1 polarizations and polarimetric parameters. This can be attributed to the high number of observations in which most of the observations (~28 000 out of ~30 000) exhibited less than 1.8 mm of cumulative precipitation in the 12 hours period prior to the S1 acquisition, as defined in (Benninga, van der Velde, and Su 2019). Although a moderate correlation was found between SAR features and temperature in this study, but only for coniferous forests, temperature was found to have a strong correlation with C-band SAR backscatter in other studies, such as in Olesk et al. (2015). Moreover, in previous studies (Rüetschi, Small, and Waser 2019; Benninga, van der Velde, and Su 2019; Ranson and Sun 2000) it was found that freezing conditions and temperatures below 1 °C cause a significant decrease in SAR backscatter over forests. Therefore, the influence of environmental factors, specifically precipitation and low temperatures, on the SAR backscatter in vegetation over time should be further examined in future studies.

Weaker correlations between SAR and optical features were found in this study (with a maximum of 0.54 between FAPAR and VH/VV) compared to previous studies, e.g. 0.63–0.84 in (Jiao, McNairn, and Dingle Robertson 2021), 0.41–0.83 in (Alvarez-Mozos et al. 2021), 0.45–0.74 in (Holtgrave et al. 2020). These studies, however, focused on agricultural areas while performing analysis only on mono-temporal image pairs, using an image-to-image comparison. A correlation of 0.77 between VV/VH and NDVI time series in broad-leaved temperate forests was found in Frison et al. (2018), while almost no correlation was found in coniferous forests. This is in line with



the findings of this study, where a significantly weaker correlation was found between optical and SAR features in coniferous forests. The variability in the individual time series (visualized with lighter lines in Fig. 5 and Fig. 6) for both SAR and optical features suggests that there is variation within both forest types, potentially due to microclimatic or topographic conditions (elevation, slope, aspect), species composition or other ecological factors (Mašek et al. 2023). The noisy behavior of optical TS throughout the year can also be attributed to insufficient haze, cloud and shadow masking.

#### 4. Conclusion

The study aimed to identify the most effective SAR polarimetric parameters for forest monitoring through quantitative and qualitative analyses for Czech forests. The analyses revealed that some of the SAR features exhibit identical behavior, providing no additional information, demonstrated a rather noisy behavior over time, or showed low performance in differentiation of forest types in time series classification. Therefore, the two original S1 polarizations (VV and VH) and two polarimetric parameters (VV/VH and VH/VV) were identified as most suitable and best performing in all the tested aspects and are proposed for further use in forest monitoring. Moreover, in a correlation analysis between SAR and optical features, the strongest correlation was found for broad-leaved forest for VV/VH and VH/VV, while the highest overall accuracy in the time series classification was achieved by VH. As a secondary output, this study introduced the MMTS-GEE tool to generate spatially and temporally aligned multi-modal time series datasets including paired S1 and S2 data, extended with DEM and weather data in GEE. The MMTS-GEE offers high flexibility for users to adopt it for various geographical areas, time frames, adjust processing pipelines or enhance the modality of the tool with additional datasets. This versatility enables its use in time series analyses, intercomparisons and in machine learning applications for tabular time series data. The data generated with MMTS-GEE were used in the case study of Czechia focusing on the identification of the most efficient SAR features for forest monitoring. The public availability of the MMTS-GEE code increases its accessibility and usability for researchers and supports further development and customization of the tool to meet specific research needs. Given its limitation to tabular data, further development of the tool for DL-ready data generation would be important.

#### Acknowledgements

This work was supported by the Charles University Grant Agency – *Grantová Agentura Univerzity Karlovy*

(GAUK) Grant No. 412722 and the European Union's Caroline Herschel Framework Partnership Agreement on Copernicus User Uptake under grant agreement No. FPA 275/G/GRO/COPE/17/10042, project FPCUP (Framework Partnership Agreement on Copernicus User Uptake). Daniel Paluba would like to thank the Erasmus+ programme for the financial support during his research stay at the  $\Phi$ -lab, European Space Agency (ESA) in Frascati, Italy.

#### References

- Alvarez-Mozos, J., Villanueva, J., Arias, M., Gonzalez-Audicana, M. (2021): Correlation Between NDVI and Sentinel-1 Derived Features for Maize. In: 2021 IEEE International Geoscience and Remote Sensing Symposium IGARSS, 6773–6776, <https://doi.org/10.1109/IGARSS47720.2021.9554099>.
- Bai, Z., Fang, S., Gao, J., Zhang, Y., Jin, G., Wang, S., Zhu, Y., Xu, J. (2020): Could Vegetation Index be Derive from Synthetic Aperture Radar? – The Linear Relationship between Interferometric Coherence and NDVI. *Scientific Reports* 10: 6749, <https://doi.org/10.1038/s41598-020-63560-0>.
- Bartels, S. F., Chen, H. Y. H., Wulder, M. A., White, J. C. (2016): Trends in Post-disturbance recovery rates of Canada's forests following wildfire and harvest. *Forest Ecology and Management* 361, 194–207, <https://doi.org/10.1016/j.foreco.2015.11.015>.
- Benninga, H.-J. F., Van Der Velde, R., Su, Z. (2019): Impacts of Radiometric Uncertainty and Weather-Related Surface Conditions on Soil Moisture Retrievals with Sentinel-1. *Remote Sensing* 11(17): 2025, <https://doi.org/10.3390/rs11172025>.
- Bey, A., Sánchez-Paus Díaz, A., Maniatis, D., Marchi, G., Mollicone, D., Ricci, S., Bastin, J.-F., Moore, R., Federici, S., Rezende, M., Patriarca, C., Turia, R., Gamoga, G., Abe, H., Kaidong, E., Miceli, G. (2016): Collect Earth: Land Use and Land Cover Assessment through Augmented Visual Interpretation. *Remote Sensing* 8(10): 807, <https://doi.org/10.3390/rs8100807>.
- Buchhorn, M., Smets, B., Bertels, L., Roo, B. D., Lesiv, M., Tsendbazar, N.-E., Herold, M., Fritz, S. (2020): Copernicus Global Land Service: Land Cover 100m: collection 3: epoch 2017: Globe. Zenodo.
- Chang, J. G., Shoshany, M., Oh, Y. (2018): Polarimetric Radar Vegetation Index for Biomass Estimation in Desert Fringe Ecosystems. *IEEE Transactions on Geoscience and Remote Sensing* 56(12), 7102–7108, <https://doi.org/10.1109/TGRS.2018.2848285>.
- Copernicus Climate Change Service (2019): ERA5-Land hourly data from 2001 to present. ECMWF.
- Curtis, P. G., Slay, C. M., Harris, N. L., Tyukavina, A., Hansen, M. C. (2018): Classifying drivers of global forest loss. *Science* 361(6407), 1108–1111, <https://doi.org/10.1126/science.aau3445>.
- De Luca, G., Silva, J. M. N., Modica, G. (2022): Regional-scale burned area mapping in Mediterranean regions based on the multitemporal composite integration of Sentinel-1 and Sentinel-2 data. *GIScience & Remote Sensing* 59(1), 1678–1705, <https://doi.org/10.1080/15481603.2022.2128251>.

- Didan, K. (2021a): MODIS/Terra Vegetation Indices 16-Day L3 Global 1km SIN Grid V061. NASA EOSDIS Land Processes Distributed Active Archive Center.
- Didan, K. (2021b): MODIS/Terra Vegetation Indices 16-Day L3 Global 250m SIN Grid V061. NASA EOSDIS Land Processes Distributed Active Archive Center.
- Didan, K., Barreto, A. (2018): VIIRS/NPP Vegetation Indices 16-Day L3 Global 500m SIN Grid V001. NASA EOSDIS Land Processes Distributed Active Archive Center.
- dos Santos, E. P., Da Silva, D. D., o Amaral, C. H. (2021): Vegetation cover monitoring in tropical regions using SAR-C dual-polarization index: seasonal and spatial influences. *International Journal of Remote Sensing* 42(19), 7581–7609, <https://doi.org/10.1080/01431161.2021.1959955>.
- Dostálová, A., Lang, M., Ivanovs, J., Waser, L. T., Wagner, W. (2021): European Wide Forest Classification Based on Sentinel-1 Data. *Remote Sensing* 13(3): 337, <https://doi.org/10.3390/rs13030337>.
- Dostálová, A., Milenkovic, M., Hollaus, M., Wagner, W. (2016): Influence of Forest Structure on the Sentinel-1 Backscatter Variation – Analysis with Full-Waveform LiDAR Data. In *Proceedings of the Living Planet Symposium, Prague, Czech Republic, 9–13 May 2016; Volume 740*, p. 202.
- Dostálová, A., Wagner, W., Milenković, M., Hollaus, M. (2018): Annual seasonality in Sentinel-1 signal for forest mapping and forest type classification. *International Journal of Remote Sensing* 39(21), 7738–7760, <https://doi.org/10.1080/01431161.2018.1479788>.
- Dufourg, C., Pelletier, C., May, S., Lefèvre, S. (2024): *Satellite Image Time Series Datasets*.
- EUROPEAN SPACE AGENCY, AIRBUS (2022): Copernicus DEM. European Space Agency.
- Fauzi, J. (2022): Time Series Classification: A review of Algorithms and Implementations. *Proud Pen*. In press, 978-1-83815241-3, hal-03558165.
- Filgueiras, R., Mantovani, E. C., Althoff, D., Fernandes Filho, E. I., Cunha, F. F. da (2019): Crop NDVI Monitoring Based on Sentinel 1. *Remote Sensing* 11(12): 1441, <https://doi.org/10.3390/rs11121441>.
- Forzieri, G., Dakos, V., Mcdowell, N. G., Ramdane, A., Cescatti, A. (2022): Emerging signals of declining forest resilience under climate change. *Nature* 608, 534–539, <https://doi.org/10.1038/s41586-022-04959-9>.
- Frison, P.-L., Fruneau, B., Kmiha, S., Soudani, K., Dufrêne, E., Le Toan, T., Koleček, T., Villard, L., Mougín, E., Rudant, J.-P. (2018): Potential of Sentinel-1 Data for Monitoring Temperate Mixed Forest Phenology. *Remote Sensing* 10(12): 2049, <https://doi.org/10.3390/rs10122049>.
- Fuster, B., Sánchez-Zapero, J., Camacho, F., García-Santos, V., Verger, A., Lacaze, R., Weiss, M., Baret, F., Smets, B. (2020): Quality Assessment of PROBA-V LAI, fAPAR and fCOVER Collection 300 m Products of Copernicus Global Land Service. *Remote Sensing* 12(6): 1017, <https://doi.org/10.3390/rs12061017>.
- Gamon, J. A., Field, C. B., Goulden, M. L., Griffin, K. L., Hartley, A. E., Joel, G., Penuelas, J., Valentini, R. (1995): Relationships Between NDVI, Canopy Structure, and Photosynthesis in Three Californian Vegetation Types. *Ecological Applications* 5(1), 28–41, <https://doi.org/10.2307/1942049>.
- Global Forest Watch (2014): *Forest Monitoring, Land Use & Deforestation Trends* | Global Forest Watch. Available online: <https://www.globalforestwatch.org/> (accessed on 16. 7. 2024).
- Gorelick, N., Hancher, M., Dixon, M., Ilyushchenko, S., Thau, D., Moore, R. (2017): Google Earth Engine: Planetary-scale geospatial analysis for everyone. *Remote Sensing of Environment* 202, 18–27, <https://doi.org/10.1016/j.rse.2017.06.031>.
- Hansen, M. C., Potapov, P. V., Moore, R., Hancher, M., Turubanova, S. A., Tyukavina, A., Thau, D., Stehman, S. V., Goetz, S. J., Loveland, T. R., Kommareddy, A., Egorov, A., Chini, L., Justice, C. O., Townshend, J. R. G. (2013): High-Resolution Global Maps of 21st-Century Forest Cover Change. *Science* 342(6160), 850–853, <https://doi.org/10.1126/science.1244693>.
- Harris, N. L., Gibbs, D. A., Baccini, A., Birdsey, R. A., De Bruin, S., Farina, M., Fatoyinbo, L., Hansen, M. C., Herold, M., Houghton, R. A., Potapov, P. V., Suarez, D. R., Roman-Cuesta, R. M., Saatchi, S. S., Slay, C. M., Turubanova, S. A., Tyukavina, A. (2021): Global maps of twenty-first century forest carbon fluxes. *Nature Climate Change* 11, 234–240, <https://doi.org/10.1038/s41558-020-00976-6>.
- Hird, J. N., Delancey, E. R., Mcdermid, G. J., Kariyeva, J. (2017): Google Earth Engine, Open-Access Satellite Data, and Machine Learning in Support of Large-Area Probabilistic Wetland Mapping. *Remote Sensing* 9(12): 1315, <https://doi.org/10.3390/rs9121315>.
- Holtgrave, A.-K., Röder, N., Ackermann, A., Erasmi, S., Kleinschmit, B. (2020): Comparing Sentinel-1 and -2 Data and Indices for Agricultural Land Use Monitoring. *Remote Sensing* 12(18): 2919, <https://doi.org/10.3390/rs12182919>.
- Huang, S., Tang, L., Hupy, J. P., Wang, Y., Shao, G. (2021): A commentary review on the use of normalized difference vegetation index (NDVI) in the era of popular remote sensing. *Journal of Forestry Research* 32, 1–6, <https://doi.org/10.1007/s11676-020-01155-1>.
- Huete, A., Didan, K., Miura, T., Rodriguez, E. P., Gao, X., Ferreira, L. G. (2002): Overview of the radiometric and biophysical performance of the MODIS vegetation indices. *Remote Sensing of Environment* 83(1), 195–213, [https://doi.org/10.1016/S0034-4257\(02\)00096-2](https://doi.org/10.1016/S0034-4257(02)00096-2).
- Jiao, X., Mcnairn, H., Dingle Robertson, L. (2021): Monitoring crop growth using a canopy structure dynamic model and time series of synthetic aperture radar (SAR) data. *International Journal of Remote Sensing* 42(17), 6433–6460, <https://doi.org/10.1080/01431161.2021.1938739>.
- Kim, Y., Van Zyl, J. (2000): On the relationship between polarimetric parameters. *GARSS 2000. IEEE 2000 International Geoscience and Remote Sensing Symposium. Taking the Pulse of the Planet: The Role of Remote Sensing in Managing the Environment. Proceedings 3*, 1298–1300 (Cat. No.00CH37120), Honolulu, HI, USA, <https://doi.org/10.1109/IGARSS.2000.858099>.
- Kosztra, B., Büttner, G., Hazeu, G., Arnold, S. (2019): Updated CLC illustrated nomenclature guidelines. European Environment Agency. Available online: [https://land.copernicus.eu/content/corine-land-cover-nomenclature-guidelines/docs/pdf/CLC2018\\_Nomenclature\\_illustrated\\_guide\\_20190510.pdf](https://land.copernicus.eu/content/corine-land-cover-nomenclature-guidelines/docs/pdf/CLC2018_Nomenclature_illustrated_guide_20190510.pdf) (accessed on 10.4.2024).

- Lee, J.-S. (1985): Speckle Suppression and Analysis for Synthetic Aperture Radar Images. Proc. SPIE 0556, Intl Conf on Speckle, <https://doi.org/10.1117/12.949537>.
- Liu, H. Q., Huete, A. (1995): A feedback based modification of the NDVI to minimize canopy background and atmospheric noise. *IEEE Transactions on Geoscience and Remote Sensing* 33(2), 457–465, <https://doi.org/10.1109/TGRS.1995.8746027>.
- Löning, M., Király, F., Bagnall, T., Middlehurst, M., Ganesh, S., Oastler, G., Lines, J., Walter, M., Viktorkaz, Mentel, L., Chrisholder, Tsaprounis, L., Rnkuhns, Parker, M., Owoseni, T., Rockenschaub, P., Danbartl, Jesellier, Eenticott-Shell, Gilbert, C., Bulatova, G., Lovkush, Schäfer, P., Khrapov, S., Buchhorn, K., Take, K., Subramanian, S., Meyer, S. M., Aidenrushbrooke, Rice, B. (2022): <https://github.com/sktime/sktime/releases> . v0.13.4. Zenodo.
- Ma, J., Li, J., Wu, W., Liu, J. (2023): Global forest fragmentation change from 2000 to 2020. *Nature Communications* 14: 3752, <https://doi.org/10.1038/s41467-023-39221-x>.
- Mandal, D., Kumar, V., Ratha, D., Dey, S., Bhattacharya, A., Lopez-Sanchez, J. M., Mcnairn, H., Rao, Y. S. (2020a): Dual polarimetric radar vegetation index for crop growth monitoring using sentinel-1 SAR data. *Remote Sensing of Environment* 247: 111954, <https://doi.org/10.1016/j.rse.2020.111954>.
- Mandal, D., Ratha, D., Bhattacharya, A., Kumar, V., Mcnairn, H., Rao, Y. S., Frery, A. C. (2020b): A Radar Vegetation Index for Crop Monitoring Using Compact Polarimetric SAR Data. *IEEE Transactions on Geoscience and Remote Sensing* 58(9), 6321–6335, <https://doi.org/10.1109/TGRS.2020.2976661>.
- Mašek, J., Tumajer, J., Lange, J., Kaczka, R., Fišer, P., Treml, V. (2023): Variability in Tree-ring Width and NDVI Responses to Climate at a Landscape Level. *Ecosystems* 26, 1144–1157, <https://doi.org/10.1007/s10021-023-00822-8>.
- May, J. L., Healey, N. C., Ahrends, H. E., Hollister, R. D., Tweedie, C. E., Welker, J. M., Gould, W. A., Oberbauer, S. F. (2017): Short-Term Impacts of the Air Temperature on Greening and Senescence in Alaskan Arctic Plant Tundra Habitats. *Remote Sensing* 9(12), 1338, <https://doi.org/10.3390/rs9121338>.
- Ministry of Agriculture of the Czech Republic (2022): Information on forests and forestry in the Czech Republic by 2021. Ministry of Agriculture of the Czech Republic.
- Mountrakis, G., Im, J., Ogole, C. (2011): Support vector machines in remote sensing: A review. *ISPRS Journal of Photogrammetry and Remote Sensing* 66(3), 247–259, <https://doi.org/10.1016/j.isprsjprs.2010.11.001>.
- Mullissa, A., Vollrath, A., Odongo-Braun, C., Slaughter, B., Balling, J., Gou, Y., Gorelick, N., Reiche, J. (2021): Sentinel-1 SAR Backscatter Analysis Ready Data Preparation in Google Earth Engine. *Remote Sensing* 13(10): 1954, <https://doi.org/10.3390/rs13101954>.
- Myneni, R., Knyazikhin, Y. (2018): VIIRS/NPP Leaf Area Index/FPAR 8-Day L4 Global 500m SIN Grid V001. NASA EOSDIS Land Processes Distributed Active Archive Center.
- Myneni, R., Knyazikhin, Y., Park, T. (2021): MODIS/Terra+Aqua Leaf Area Index/FPAR 4-Day L4 Global 500m SIN Grid V061. NASA EOSDIS Land Processes Distributed Active Archive Center. Available online: <https://doi.org/10.5067/VIIRS/VNP15A2H.001> (accessed on 5.4.2024).
- Nicolau, A. P. (2024): Cloud Score+ in Action: Land Cover Mapping in Ecuador, Google Earth and Earth Engine. Available online: <https://medium.com/google-earth/cloud-score-in-action-land-cover-mapping-in-ecuador-fd1c5c424317> (accessed on 26. 4. 2024).
- Olesk, A., Voormansik, K., Põhjala, M., Noorma, M. (2015): Forest change detection from Sentinel-1 and ALOS-2 satellite images. *IEEE 5th Asia-Pacific Conference on Synthetic Aperture Radar (APSAR)*, 522–527, <https://doi.org/10.1109/APSAR.2015.7306263>.
- Oliveira, W. V. De, Dutra, L. V., Sant'anna, S. J. S. (2023): A Comparison Of Multi-Class Svm Strategies And Kernel Functions For Land Cover Classification. Available online: <https://proceedings.science/sbsr-2023/trabalhos/a-comparison-of-multi-class-svm-strategies-and-kernel-functions-for-land-cover-c?lang=en> (accessed on 17. 4. 2024).
- Onáčillová, K., Křištofová, V., Paluba, D. (2023): Automatic forest cover classification using Sentinel-2 multispectral satellite data and machine learning algorithms in Google Earth Engine. *Acta Geographica Universitatis Comenianae* 67(2), 163–185.
- Paluba, D., Laštovička, J., Mouratidis, A., Štych, P. (2021): Land Cover-Specific Local Incidence Angle Correction: A Method for Time-Series Analysis of Forest Ecosystems. *Remote Sensing* 13(9): 1743, <https://doi.org/10.3390/rs13091743>.
- Paluba, D., Papale, L. G., Perivolioti, T.-M., Štych, P., Laštovička, J., Kalaitzis, P., Karadimou, G., Papageorgiou, E., Mouratidis, A. (2023): Unsupervised Burned Area Mapping in Greece: Investigating the Impact of Precipitation, Pre- and Post-Processing of Sentinel-1 Data in Google Earth Engine. *IGARSS 2023 – 2023 IEEE International Geoscience and Remote Sensing Symposium*, Pasadena, CA, USA, 2520–2523, <https://doi.org/10.1109/IGARSS52108.2023.10283130>.
- Pasquarella, V. (2024): All Clear with Cloud Score+, Google Earth and Earth Engine. Available online: <https://medium.com/google-earth/all-clear-with-cloud-score-bd6ee2e2235e> (accessed on 26. 4. 2024).
- Pasquarella, V. J., Brown, C. F., Czerwinski, W., Rucklidge, W. J. (2023): Comprehensive quality assessment of optical satellite imagery using weakly supervised video learning. *IEEE/CVF Conference on Computer Vision and Pattern Recognition Workshops (CVPRW)*, Vancouver, BC, Canada, 2125–2135, <https://doi.org/10.1109/CVPRW59228.2023.00206>.
- Periasamy, S. (2018): Significance of dual polarimetric synthetic aperture radar in biomass retrieval: An attempt on Sentinel-1. *Remote Sensing of Environment*, 217, 537–549, <https://doi.org/10.1016/j.rse.2018.09.003>.
- Pinheiro, M., Miranda, N., Recchia, A., Cotrufo, A., Franceschi, N., Piantanida, R., Schmidt, K., Gisinger, C., Hajduch, G., Vincent, P. (2022): Sentinel-1 instruments status and product performance update for 2022. In: *EUSAR 2022; 14th European Conference on Synthetic Aperture Radar*, 1–5.
- Ranson, K. J., Sun, G. (2000): Effects of environmental conditions on boreal forest classification and biomass estimates with SAR. *IEEE Transactions on Geoscience*



- and Remote Sensing 38(3), 1242–1252, <https://doi.org/10.1109/36.843016>.
- Reiche, J., Mullissa, A., Slagter, B., Gou, Y., Tsendbazar, N.-E., Odongo-Braun, C., Vollrath, A., Weisse, M. J., Stolle, F., Pickens, A., Donchyts, G., Clinton, N., Gorelick, N., Herold, M. (2021): Forest disturbance alerts for the Congo Basin using Sentinel-1. *Environmental Research Letters* 16(2): 024005, <https://doi.org/10.1088/1748-9326/abd0a8>.
- Richards, J. A. (2009): *The Imaging Radar System In: Remote Sensing with Imaging Radar. Signals and Communication Technology*. Springer, Berlin, Heidelberg, [https://doi.org/10.1007/978-3-642-02020-9\\_1](https://doi.org/10.1007/978-3-642-02020-9_1).
- Rüetschi, M., Small, D., Waser, L. (2019): Rapid Detection of Windthrows Using Sentinel-1 C-Band SAR Data. *Remote Sensing* 11(2): 115, <https://doi.org/10.3390/rs11020115>.
- Saatchi, S. (2019): SAR Methods for Mapping and Monitoring Forest Biomass. In: *SAR Handbook: Comprehensive Methodologies for Forest Monitoring and Biomass Estimation*. NASA. Available online: <https://ntrs.nasa.gov/api/citations/20190002563/downloads/20190002563.pdf> (accessed on 10.4.2024).
- Sahadevan, D. K., Sitiraju, S., Sharma, J. (2013): Radar Vegetation Index as an Alternative to NDVI for Monitoring of Soyabean and Cotton. In: *Indian Cartographer*. Jodhpur, 91–96.
- Schmitt, M., Ahmadi, S. A., Xu, Y., Taşkin, G., Verma, U., Sica, F., Hänsch, R. (2023): There Are No Data Like More Data: Datasets for deep learning in Earth observation. *IEEE Geoscience and Remote Sensing Magazine* 11(3), 63–97, <https://doi.org/10.1109/MGRS.2023.3293459>.
- Senf, C., Seidl, R. (2021): Mapping the forest disturbance regimes of Europe. *Nature Sustainability* 4, 63–70, <https://doi.org/10.1038/s41893-020-00609-y>.
- Smets, B., Cai, Z., Elkund, L., Tian, F., Bonte, K., Van Hoost, R., Van De Kerchove, R., Adriaensen, S., De Roo, B., Jacobs, T., Swinnen, E. (2023): High resolution vegetation phenology and productivity (HR-VPP), Daily Raw Vegetation Indices. European Union, Copernicus Land Monitoring Service 2021, European Environment Agency (EEA).
- Thanh Noi, P., Kappas, M. (2018): Comparison of Random Forest, k-Nearest Neighbor, and Support Vector Machine Classifiers for Land Cover Classification Using Sentinel-2 Imagery. *Sensors* 18(1): 18, <https://doi.org/10.3390/s18010018>.
- Turubanova, S., Potapov, P. V., Tyukavina, A., Hansen, M. C. (2018): Ongoing primary forest loss in Brazil, Democratic Republic of the Congo, and Indonesia. *Environmental Research Letters* 13: 074028, <https://doi.org/10.1088/1748-9326/aacd1c>.
- Tyukavina, A., Potapov, P., Hansen, M. C., Pickens, A. H., Stehman, S. V., Turubanova, S., Parker, D., Zalles, V., Lima, A., Kommareddy, I., Song, X.-P., Wang, L., Harris, N. (2022): Global Trends of Forest Loss Due to Fire From 2001 to 2019. *Frontiers in Remote Sensing* 3: 825190, <https://doi.org/10.3389/frsen.2022.825190>.
- Vreugdenhil, M., Wagner, W., Bauer-Marschallinger, B., Pfeil, I., Teubner, I., Rüdiger, C., Strauss, P. (2018): Sensitivity of Sentinel-1 Backscatter to Vegetation Dynamics: An Austrian Case Study. *Remote Sensing* 10(9): 1396, <https://doi.org/10.3390/rs10091396>.
- Wang, W. K., Chen, I., Hershkovich, L., Yang, J., Shetty, A., Singh, G., Jiang, Y., Kotla, A., Shang, J. Z., Yerrabelli, R., Roghanizad, A. R., Shandhi, M. M. H., Dunn, J. (2022): A Systematic Review of Time Series Classification Techniques Used in Biomedical Applications. *Sensors* 22(20): 8016, <https://doi.org/10.3390/s22208016>.
- Weiss, M., Baret, F. (2016): S2ToolBox Level 2 Products: LAI, FAPAR, FCOVER. Version 1.1.
- WMO, United Nations Educational, S., C. O. (UNESCO), Programme (UNEP), U. N. E., SCIENCE (ICSU), I. C. for (2011): Systematic Observation Requirements for Satellite-based Products for Climate Supplemental details to the satellite-based component of the Implementation Plan for the Global Observing System for Climate in Support of the UNFCCC. Available online: <https://library.wmo.int/records/item/48411-systematic-observation-requirements-for-satellite-based-products-for-climate-supplemental-details-to-the-satellite-based-component-of-the-implementation-plan-for-the-global-observing-system-for-climate-in-support-of-the-unfccc> (accessed on 12. 9. 2023).
- Zanaga, D., Van De Kerchove, R., Daems, D., De Keersmaecker, W., Brockmann, C., Kirches, G., Wevers, J., Cartus, O., Santoro, M., Fritz, S., Lesiv, M., Herold, M., Tsendbazar, N.-E., Xu, P., Ramoino, F., Arino, O. (2022): ESA WorldCover 10 m 2021 v200, <https://doi.org/10.5281/zenodo.7254221>.
- Zeng, Y., Hao, D., Huete, A., Dechant, B., Berry, J., Chen, J. M., Joiner, J., Frankenberg, C., Bond-Lamberty, B., Ryu, Y., Xiao, J., Asrar, G. R., Chen, M. (2022): Optical vegetation indices for monitoring terrestrial ecosystems globally. *Nature Reviews Earth & Environment* 3, 477–493, <https://doi.org/10.1038/s43017-022-00298-5>.